Growth of isolated and embedded Cu-containing chalcopyrite clusters and nanocrystals by dry processing

D. Fuertes Marrón,* S. Lehmann, and M. Ch. Lux-Steiner
Department of Solar Energy, Hahn-Meitner Institut, Glienicker Str. 100, 14109 Berlin, Germany
(Received 10 July 2007; revised manuscript received 5 October 2007; published 21 February 2008)

A dry method for the growth of Cu-containing chalcopyrite nanocrystals on solid substrates is described. The experimental realization of the method relies on decoupling, by means of metal precursors, the two main issues of the growth of highly structured material: on the one hand, the structuring itself of the target material at the desired scale, and on the other hand, the actual chemical process ensuring the quality of the material. In the present approach, the precursors, consisting of species to be incorporated during the process in the final semiconducting compound, control the *structuring*, whereas chemical vapor deposition methods account for the *chemistry* of the process. The method proposed has been analyzed at a theoretical level by means of thermochemical calculations, which helped determine the ranges of interest of the experimental parameters involved in the deposition process. By choosing different distributions of Cu precursor deposited on standard glass substrates, nanocrystals, submicrometer polycrystalline dots, or macroscopic clusters of Cu-containing chalcopyrite compounds have been grown, either as isolated units or, alternatively, as embedded structures in a matrix of a binary chalcogenide compound, as a function of processing parameters. Compositional and structural analyses were used to determine the nature of the crystalline phases obtained thereof. Scanning probe techniques were used to characterize the samples at nanometer scale, demonstrating the suitability of the proposed method.

DOI: 10.1103/PhysRevB.77.085315 PACS number(s): 81.07.−b

I. INTRODUCTION

Within the field of thin-film photovoltaics, Cu-containing chalcopyrites of the type $Cu(In,Ga)(S,Se)_2$ have demonstrated superior performance among currently available technologies, including those based on Si and CdTe.[1] Standard methods for the growth of chalcopyrite thin films, such as physical evaporation, chemical transport, or rapid thermal processing, result in closed and laterally homogeneous layers, allowing rapid and easy further processing steps for the fabrication of solar cells.[2] However, chalcopyrites have unique properties, such as high absorption coefficients, complex valence band structures, and forgiving defect chemistries, which make them highly interesting, not only in the field of large-area photovoltaics but also in branches of microelectronics including spintronics,[3] lasers,[4] light-emitting diodes,[5] magnetic semiconductors,[6] and nonlinear optical devices,[7] among others. In all these fields and partly in contrast to the requirements of conventional photovoltaics mass production, patterning and lateral structuring at reduced dimensions are commonplace. Even within the field of photovoltaics, the ability to implement high-structuring schemes of active materials might be relevant for the realization, e.g., of point contacts, passivation approaches, or new cell designs including nanostructures.

The growth of nanostructured chalcopyrite materials is therefore receiving increasing attention. The goal is to exploit those properties related to reduced dimensions and electronic confinement, adding them up to the palette of intrinsic material properties exhibited by these compounds. With this aim, a number of routes have been explored for the preparation of highly structured Cu-containing chalcopyrites, including metal-induced growth[8,9] and wet processes,[10–14] among others. These processes can provide a variety of forms and *nanoshapes* of the target materials, such as whiskers, nanorods, nanocubes, and nanowires. However, these are, in most cases, *ad hoc* procedures that offer limited control over the fine structure of these geometries (such as length, size, or density) and appear to be *exclusive*, in the sense that they do not allow for the eventual combination of two or more of those geometries in a single growth process.

In this paper, we propose a method for the growth of nanocrystals and highly structured chalcopyrite materials of the type $Cu(In,Ga)(S,Se)_2$ based on the utilization of metal precursors.[15] The growth of highly structured materials can be considered, in general terms, as a twofold problem:[16] on the one hand, the chemical reaction process of choice must lead to the formation of the target material, and on the other hand, the structuring must be achieved at the desired size scale. The use of precursors appears advantageous over alternative methods, such as postgrowth patterning, in as much as the precursor effectively controls one of the two aspects mentioned above. In the proposed approach, the metal precursor is responsible for the size and distribution of the chalcopyrite crystals, i.e., for the *structuring*, whereas the growth process controls the material quality of the structures, in this terminology, the *chemistry*.

II. EXPERIMENTAL DETAILS

Cu dots with dimensions ranging from the nanometer scale (in the form of nanoparticles) up to macroscopic structures (millimeter-sized clusters of polycrystalline material) to be used as metal precursors were evaporated on Mo-coated soda-lime glass substrates. The evaporation process ran just for a few seconds, in order to provide a fairly random lateral distribution of Cu particles, while avoiding the formation of a closed Cu overlayer. Scanning electron microscopy (SEM)

 ©2008 The American Physical Society

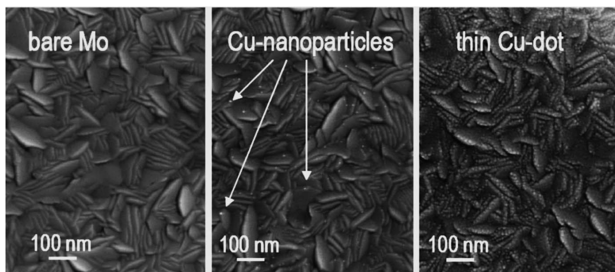

FIG. 1. SEM top views of substrates used in this study: (left) bare Mo-coated soda-lime glass: and (center and right) Cu particles (tiny white dots) deposited on Mo after different evaporation times, typically a few seconds. The image on the right was obtained at the center of a Cu dot (0.5 mm diameter), evaporated on Mo using a circular mask; off the dot, the substrate appearance is that of the image on the left.

images of such precursors, obtained with a LEO Gemini system equipped with a field emission gun, are shown in Fig. 1. More sophisticated methods for the deposition of the precursors, providing fine control over the size distribution and lateral ordering, are abundant in the literature and may fulfil certain requirements for specific applications. These aspects, however, are not included in the present discussion, which is focused on the proof of concept.

The substrates with precursors were subsequently introduced in an open-tube chemical vapor deposition (CVD) reactor and exposed to a reactive gas atmosphere containing Ga and Se in the form of $GaCl_x$ and H_2Se.[8] Halogen-supported CVD is a suitable process for the realization of the proposed approach, as it not only allows the volatilization of metallic species at moderate temperatures but also offers precise control over the reactive gas flows and hence over the supersaturation conditions holding on the substrate side, leading to deposition. The reactive gaseous mixture was provided from Ga_2Se_3 powder (source material, synthesized from the elements), swept by a continuous flow of HCl (transport gas) diluted in H_2 (carrier gas), typically at a ratio of 1:10 or higher. The temperature at the source was kept constant at 600 °C and the reactor pressure at 100 mbar. Additional experiments were carried out in a similar fashion with different binary chalcogenide sources, namely, Ga_2S_3, In_2S_3, and In_2Se_3, demonstrating the suitability of the approach for the entire family of $Cu(In,Ga)(S,Se)_2$ compounds.

Thermochemical calculations were performed in order to simulate the reactions taking place in the CVD reactor and to predict the range of interest of the experimental parameters to be used for the proposed growth method. The calculations were carried out with the software package CHEMSAGE.[17] The expected amount of species under thermodynamical equilibrium was calculated as a function of the incoming amount of reactants, temperature, and pressure by minimizing the free energy of the system, starting from available thermochemical data [molar entropies, enthalpies of formation, and coefficients of heat capacity (see Table I)] of the compounds expected to participate in the reactions.[18,19]

X-ray diffraction (Bruker, Cu $K\alpha$ emission operated at 40 mA and 40 kV) was used to determine the nature of the crystalline phases present on the substrates. A scanning tunneling microscope (VT-UHV, Omicron) was employed to characterize samples at room temperature with lateral resolution in the nanometer range.

III. APPROACH

As for any conventional CVD-based process, the effective volatilization and deposition of material for given values of temperature T and pressure p can be satisfactorily described from the unbalance of the chemical potential of the different species contained in the gas and the solid phases, according to $\Delta\mu=\mu_{gas}-\mu_{solid}$.[20] For $\Delta\mu>0$, deposition from the gas in the solid phase proceeds; for $\Delta\mu<0$, volatilization occurs. These conditions follow naturally from the definition of the chemical potential as the change in Gibb's free energy with the number of particles of the given species: the phase with the higher chemical potential for given values of temperature and pressure (i.e., in thermodynamical equilibrium) is unstable against the phase with the lower chemical potential. Maintaining the supersaturation under quasistatic conditions on the deposition side, with well defined values of temperature and pressure, either p or T can be used as free parameter determining the chemical potential, while keeping the other parameter fixed at a certain value. For constant p, $\mu=\mu(T)$, and the conditions establishing either volatilization or deposition can be set by adjusting different temperatures T and T'. The presence of finite and laterally inhomogeneous precursors on the substrate exposed to the reactive gas introduces lateral variations in the chemical potential inequalities, as schematically shown in Fig. 2. The system $CuGaSe_2$ has been chosen in the figure as an example, with Cu dots as precursor and Ga- and Se-containing reactive gases accounting for the $GaCl_x$ and H_2Se as in the experiment. Whereas the chemical potentials corresponding to the species in the gas phase (dotted lines) can be considered constant over the entire substrate area (provided constant temperature T_{sub}, pressure, and quasistatic conditions under laminar flow hold), the same is not true for the chemical potential of solid phases. If chemical reactions are allowed between the precursor and the species in the gas phase, the values of the corresponding chemical potential in the solid phases will be those of the final products, i.e., different from those corresponding to the direct deposition of the species from the gas into the solid phase. This lateral variation of the chemical potential in the solid phases containing gallium and selenium, which critically depends on the lateral size of the precursor, is represented by $\mu^{solid}_{Ga,Se}(T_{sub})$ in the figure (solid lines). The relative change $\Delta\mu$ in the values of $\mu^{solid}_{Ga,Se}(T_{sub})$ represents the difference in chemical potential between the solid phases for the given conditions. These variations are responsible for the selective deposition in the solid phase (hatched areas in the figure) of either isolated structures at those spots where the precursor was located, or alternatively, as the simultaneous occurrence of reactions in the solid phase at and off the precursor, in a single process. The result of such process is the formation of autoarranged ternary compounds, either as isolated or, alternatively, as embedded structures in a matrix of a different semiconducting com-

TABLE I. Selected thermochemical parameters used in this study. General references (Refs. 18 and 19) have been updated in some cases according to experimental values (Ref. 21). $\Delta_f H^0$ standard enthalpy of formation at 298.15 K; S^0 standard entropy at 298.15 K; a, b, c, d coefficients of heat capacity following $C_p = a + b \times 10^{-3} T + c \times 10^6 T^{-2} + d \times 10^{-6} T^2$, with the corresponding units as given in the table; T_{max} maximum temperature of applicability.

	$\Delta_f H^0$ (kJ mol^{-1})	S^0 (J K^{-1} mol^{-1})	a (J K^{-1} mol^{-1})	b (kJ K^{-2} mol^{-1})	c (10^{-6} J K mol^{-1})	d (10^6 J K^{-3} mol^{-1})	T_{max} (K)
Cl_2(g)	0	223.022	36.60	1.080	−0.272	0	2000
Cu	0	33.124	24.116	5.371	−0.107	−0.082	1357
CuCl(s)	−138.138	87.069	88.239	−60.021	−2.277	43.597	703
CuCl(l)	10.23		66.97	0	0	0	1485
CuCl(g)	100.409	284.213	37.293	0.54	−0.195	0	2000
$CuCl_2$	−205.951	108.137	67.274	3.004	−0.261	−15.882	766
CuH(g)	274.888	196.468	30.836	3.766	−0.0456	0	2000
CuSe	−41.84	78.241	54.81	0	0	0	326
CuSe	1.38		62.76	0	0	0	650
CuSe(g)	309.616	264.747	37.359	0.033	−0.113	0	2000
Cu_2Se	−65.260	129.682	58.576	77.404	0	0	395
Cu_2Se	6.819		84.1	0	0	0	800
$CuGaSe_2$	−250.60	160.87	117.15	4.121	−1.674	0	1363
Ga	0	40.827	26.196	0	0	0	303
Ga(l)	5.589		24.384	2.293	0.310	0	700
GaCl(g)	−80.826	240.216	37.217	0.661	−0.151	0	2000
$GaCl_2$(g)	−241.249	301.022	57.589	0.435	−0.406	0	2000
$GaCl_3$	−524.673	135.143	118.407	0	0	0	351
$GaCl_3$(l)	11.506		128.03	0	0	0	474
$GaCl_3$(g)	−422.881	325.147	82.425	0.444	−0.678	0	2000
GaSe	−159.068	70.325	44.66	12.977	0	0	1233
Ga_2Se(g)	20.930	298.880	56.030	0.115	−0.925	0	2000
Ga_2Se_3	−406.042	194.230	105.780	35.330	0	0	1293
H_2(g)	0	130.645	26.874	3.585	0.105	0	3000
HCl(g)	−92.301	186.863	26.52	4.600	0.109	0	2000
H_2Se(g)	29.302	218.928	31.772	14.651	−0.130	0	2000
Se	0	42.279	17.90	25.116	0	0	493
Se(l)	5.860		35.16	0	0	0	600
Se_6(g)	135.208	433.711	132.968	0.067	−0.593	0	2000
$SeCl_2$(g)	−33.488	295.741	57.976	0.134	−0.395	0	2000
Se_2Cl_2(g)	−21.767	353.968	82.422	1.536	−0.453	0	1000

pound, typically the binary chalcogenide used as source. The approach can be easily extended to the growth of multinary compounds, with or without a multinary matrix, by including different species at the precursor and/or in the reactive gas.

IV. RESULTS

A. Thermochemical calculations

The proposed approach for the growth of highly structured ternary and multinary compounds has been studied thermochemically considering equilibrium conditions. In order to simplify the numerical work, the chemical reactions involved in the CVD process were divided into two parts, namely, those taking place at the source side (volatilization) and those occurring at the substrate side (deposition). The products obtained from the simulations at the source side were subsequently used as reactants at the deposition side, following the approach of Meyer.[19] Figure 3(A) shows the results of the calculations simulating the volatilization of solid Ga_2Se_3 by HCl and H_2 at 600 °C and 100 mbar. According to these results, varying equilibrium amounts of H_2Se and $GaCl_x$ ($1 < x < 3$) are to be expected as a function of the incoming HCl flow (represented between 0.05 and 50 mol). Ga_2Se_3 and H_2 were provided in excess, considered not to limit the reactions (5 and 500 mol, respectively, the former not fully volatilized, as in the experiments). These results are in good agreement with those reported earlier.[19] The formation of gallium monochloride, dichloride, and trichloride [dotted lines in Fig. 3(A)] depends sensitively on

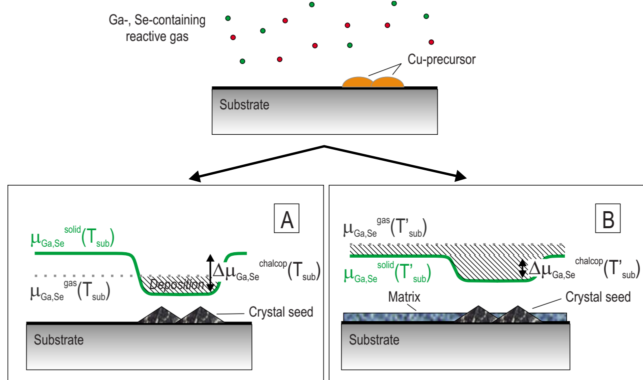

FIG. 2. (Color online) Schematics of the general method employed for the growth of chalcopyrite nanocrystals, example of $CuGaSe_2$. The size and distribution of metal precursor particles determine the size and distribution of the crystallites. For a given pressure p, the condition for the growth of isolated clusters (A, left) of ternary compound, which follows from the inequality $\mu_{\mathrm{Ga,Se}}^{gas}(T_{sub}) > \mu_{\mathrm{Ga,Se}}^{solid}(T_{sub})$, where $\mu_{\mathrm{Ga,Se}}^{gas}$ and $\mu_{\mathrm{Ga,Se}}^{solid}$ refer, respectively, to all gaseous and solid species containing gallium and selenium, should hold locally at the precursor for net deposition (hatched areas), whereas $\mu_{\mathrm{Ga,Se}}^{gas}(T_{sub}) < \mu_{\mathrm{Ga,Se}}^{solid}(T_{sub})$ must be preserved elsewhere in order to avoid further reactions in the solid phase. By the same argument, the conditions for the growth of chalcopyrite dots embedded in a matrix formed from the elements contained in the gas phase requires $\mu_{\mathrm{Ga,Se}}^{gas}(T'_{sub}) > \mu_{\mathrm{Ga,Se}}^{solid}(T'_{sub})$ to hold all over the substrate at a certain temperature T'_{sub}. Local differences still exist in $\mu_{\mathrm{Ga,Se}}^{solid}(T'_{sub})$ for the different solid phases that do or do not contain the precursor as constituent, as shown in B, right.

the amount of HCl provided, the sum of all three species (solid+open diamonds curve) following the same dependence as H_2Se (solid+open circles).

The products at the volatilization side for a given incoming amount of 50 mol HCl were then used as reactants at the substrate side, kept at 100 mbar, but sweeping the temperature between 300 and 550 °C. The results are presented in Fig. 3(B), essentially simulating the backreaction in the solid phase of Ga_2Se_3, as calculated in the previous simulation, now for different temperatures. In the context of the growth mechanism described before, this case accounts for the direct deposition of the chemical species contained in the gas phase off the precursor, i.e., for the deposition of the embedding matrix schematically shown in Fig. 2. The deposition of solid Ga_2Se_3 is predicted to occur between 300 and 530 °C, being limited in this temperature range by the availability of H_2Se. At higher temperatures, however, gaseous gallium chlorides of different stoichiometries compete with the deposition of the metal chalcogenide, becoming the most stable Ga-containing phases above 530 °C. This temperature does thus mark the upper limit for the onset of the embedding semiconductor matrix during the growth of the ternary chalcopyrite structures. The deposition of the embedding matrix is, on the other hand, inhibited in processes carried out at higher substrate temperatures.

The chemical reactions taking place at the deposition side in the presence of Cu precursors were also simulated using the available amount of copper as independent variable and the same reactants as for the previous case for two different temperatures at 100 mbar. The results are shown in Fig. 3(C). Calculating as a function of the amount of Cu permits not only to study the impact of the total mass of the precursor but also (to some limited qualitative extent) the kinetics of the process, strictly speaking not accessible from equilibrium calculations. Previous experimental results have shown that the formation of $GaSe_2$ by exposing Cu precursors to gaseous $GaCl_x$ and H_2Se in a CVD-based process is possible and that this reaction includes the formation of intermediate phases, primarily $Cu_{2-x}Se$.[22] Further exposure of stoichiometric $CuGaSe_2$ chalcopyrite to $GaCl_x$ and H_2Se leads in turn to the formation of Cu-poor phases of the type $CuGa_3Se_5$ and $CuGa_5Se_8$,[23] not included in the thermochemical calculations presented here due to the lack of reliable data in the literature, but expected to occur between $CuGaSe_2$ and Ga_2Se_3 in the results discussed later on. After consuming the

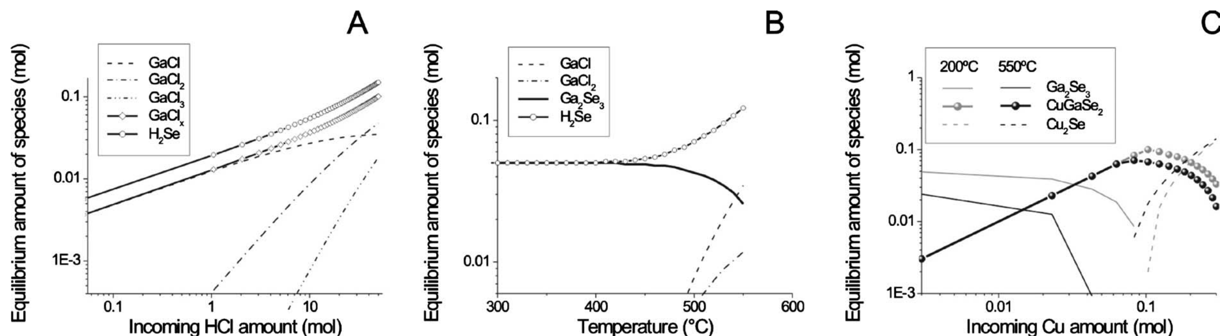

FIG. 3. (A, left) Thermochemical calculations of the equilibrium amount of species at the source side, where the (partial) volatilization of 5 mol Ga_2Se_3 proceeds at 600 °C when exposed to 500 mol H_2 and a varying amount of HCl. The line $GaCl_x$ represents the sum of the gallium monochloride, dichloride, and trichloride. (B, center) Expected amount of species at equilibrium at the substrate side as a function of temperature, when no Cu is available for reacting with the gases (input parameters from case A, calculated for 50 mol HCl), basically the case of the backreaction of case A. (C, right) The same as in B but for the case of Cu precursor being present at the substrate for two different temperatures (200 °C, dotted and 550 °C, solid) and varying Cu availability. The range of existence of single-phase chalcopyrite, already expected to form at 200 °C, is widened by increasing the temperature, mainly by inhibition of Ga_2Se_3. Competing binary chalcogenides Cu_2Se and Ga_2Se_3 dominate under excess Cu and Ga, respectively. The pressure in all cases kept at 100 mbar.

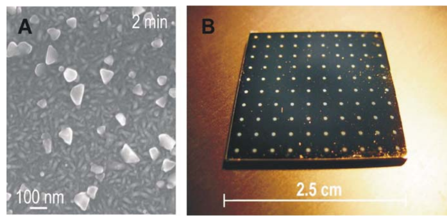

FIG. 4. (Color online) (A, left) Top view scanning electron micrograph (SEM) of $CuGaSe_2$ nanocrystals grown from Cu precursors onto Mo-coated soda-lime glass. The contrast in the background stems from the Mo texture and the processing time was 2 min at $T_{substrate}=530$ °C. (B, right) Macroscopic $CuGaS_2$ polycrystalline dots grown on Mo-coated soda-lime glass for 20 min at the same temperature. The Cu precursor was previously evaporated through a circular mask.

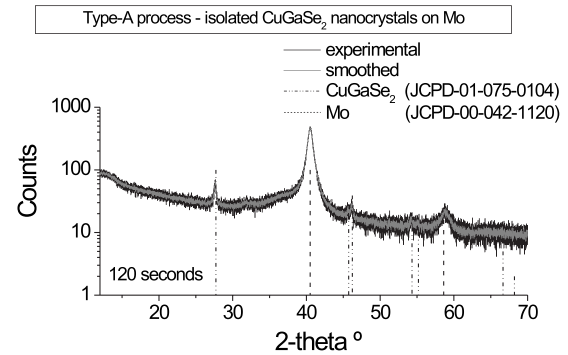

FIG. 5. XRD diffractogram obtained in grazing incidence (0.7°) of the sample shown in Fig. 4(A) and the corresponding assignment of the peaks

finite amount of Cu present in the initial precursor, the only stable solid phase expected is Ga_2Se_3. Therefore, the abscissa in Fig. 3(C) can also be considered as a temporal axis (in arbitrary units) in opposite direction to that corresponding to the provision of Cu for a given amount of initial precursor. The solid phases expected at 200 °C on the substrate side are shown by gray lines and indicate the formation of single-phase $CuGaSe_2$ in a relatively narrow range between 0.08 and 0.1 mol Cu for the set of parameters used. Excess Cu is accommodated by forming Cu_2Se, whereas excess Ga leads to the coexistence of $CuGaSe_2$ and Ga_2Se_3 as solid phases. By increasing the temperature of the substrate up to 550 °C (black lines in the figure), the window for the deposition of single-phase chalcopyrite is widened, primarily by the inhibition of Ga_2Se_3 as competing phase, for low Cu amounts, in agreement with the results obtained for the previous case of the precursor. Minor changes were recorded for the expected amounts of $CuGaSe_2$ and Cu_2Se at the Cu-rich regime, being, however, potentially relevant for a fine compositional tuning of the product. The proposed approach for the growth of highly structured material, including the cases of isolated or embedded structures in a single process as a function of the processing parameters was, thus, supported by thermochemical calculations.

B. Sample characterization

These theoretical results have been reproduced experimentally with the open-tube CVD system. As an example of a process of the type A in Fig. 2, Fig. 4(A) shows a scanning electron micrograph (top view) of a few isolated nanocrystals of $CuGaSe_2$, grown on Mo-coated soda-lime glass for 2 min at $T_{sub}=530$ °C. X-ray diffraction (XRD) analysis under grazing incidence of 0.7° showed no evidence of additional crystalline phases other than $CuGaSe_2$ and Mo (see Fig. 5). The lateral dimensions of the crystallites lie below 100 nm, although distributed in size, as the original precursors. Pseudotriangular shaped {112} facets terminate the crystals, showing a characteristic tetragonal disphenoid habitus.[24] The typical texture of bare Mo is responsible for the background contrast.

Up scaling the dimensions of the precursors acting like seeds lead to larger clusters of the target material, according to the design rules proposed earlier: the precursor controls the final size and spatial distribution, whereas the reactive gas process controls the chemistry of the growth. Figure 4(B) shows one example, for which Cu dots of 0.5 mm diameter were evaporated using a circular mask onto Mo-coated soda-lime glass. In this case, sulfides were tested using Ga_2S_3 as source material. The CVD process proceeded for 20 min, other parameters as for the case of the selenide presented above. The final product was an array of polycrystalline dots of $CuGaS_2$, an interesting material for the fabrication of light-emitting diodes.[5] The lateral selectivity for the onset of the growth only at those spots targeted by the presence of precursors allows for periodic arrangements of active material. This issue facilitates eventual further processing steps, for example, those leading to the fabrication of photodiode arrays or the implementation of point contacts for chalcopyrite-based devices.

Further examples of this type of growth are shown in Fig. 6 for different chalcopyrite compounds. Images on the right show single chalcopyrite dots obtained from the transport of In_2S_3 (top), Ga_2S_3 (middle), and Ga_2Se_3 (lower) on Cu precursors of the same type as in Fig. 4(B). The same reaction conditions were held in all cases, with a substrate temperature of 530 °C for 20 min deposition. Rectangular marks in Fig. 6 correspond to enlarged areas zoomed in on the left part of the image. Each compound shows a distinct fine structure, characterized by a size distribution of the crystallites forming the dots. In the case of clusters obtained from the transport of In_2S_3 (upper panel), the dot is formed by a dense and fairly homogeneous distribution of nanocrystallites, visible at largest magnification as background, on top of which large crystallites well above a micrometer in length appear distributed randomly in the inner part of the dot. A characteristic annular geometry appears at the edge of the dot, formed by a double ring of large crystallites, identical to those at the inner part of the dot. The irregular shape of the large crystallites seems to result from the coalescence of smaller grains, though maintaining sharp edges and flat surface terminations that allow identify in most cases the typical tetragonal disphenoid geometries of the individual crystals. A similar distribution of crystallite sizes shows up in the case of Ga_2S_3 on Cu (middle panel), where the annular geometry, composed in this case of several rings, is already evident from the overview picture on

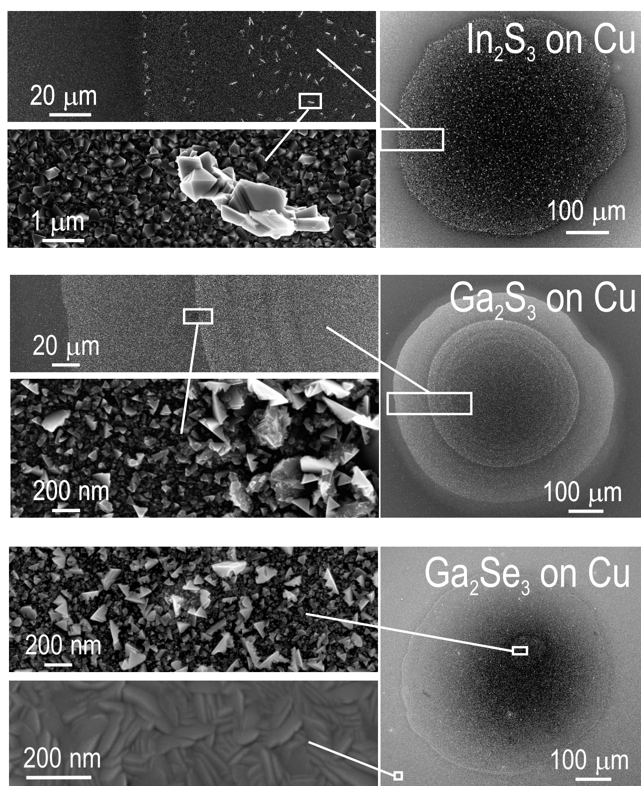

FIG. 6. SEM top views obtained at different magnifications (zooming into the marked areas) of macroscopic chalcopyrite dots grown from different binary chalcogenides. (Upper panel) $CuInS_2$ obtained from the transport of In_2S_3 on Cu precursors, with a fairly random distribution of large irregular crystallites in the inner part of the dot and a double outer ring at the dot edge. In the case of $CuGaS_2$ (center), a characteristic annular distribution of crystallite size is evident. $CuGaSe_2$ (lower panel) shows a rather homogeneous distribution of crystallite size, with similar crystal habitus as for $CuGaS_2$. In all cases, the surface of the Mo coating serving as substrate appears clean off the dots (lower inset). All samples were processed under identical reactor conditions at $T_{sub}=530$ °C.

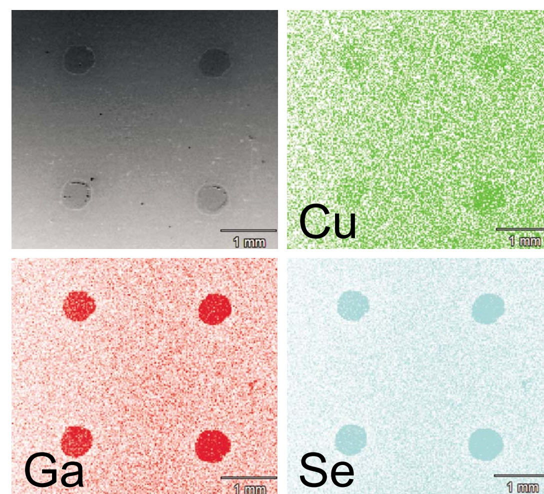

FIG. 7. (Color online) SEM picture (upper left) and corresponding EDX mappings of Cu, Ga, and Se L lines of the $CuGaSe_2$ dot sample of Fig. 6.

the right. Zooming in at the ring edges reveals a rather abrupt frontier in the size distribution, as shown in the picture of largest magnification. Also in this case, larger crystallites seem to be formed from coalescence of smaller grains, though a characteristic crown-shaped morphology appears in some cases. This geometry has been observed in Ga-rich $CuGaSe_2$ samples grown by chemical transport methods and has been ascribed to repeated twinning around ⟨110⟩ direction that leaves equivalent {112} surfaces terminating the twin crystals rotated 180° with respect to each other.[23] The resulting disphenoid structures conform a quasisixfold geometry, where each structure appears, like the teeth of a saw, rotated by ≈60° with respect to its neighbors.

The distribution of grain size in samples obtained from the transport of Ga_2Se_3 on Cu is more homogeneous than in the cases of sulfide compounds, as shown in the lower panel of Fig. 6. No evidences of crystallites larger than a micrometer in length were found, though the characteristic geometry of Ga-rich samples discussed before is also present here, with larger crystallites at the upper part of the dot lying over a dense background of smaller crystallites. Figure 7 shows compositional mappings at a lower magnification obtained by energy dispersive x-ray (EDX) analysis of L lines of Cu, Ga, and Se of the same sample, in which four dots are visible in the corresponding SEM picture (upper left). The scale bar represents 1 mm. Differences observed in the distribution and shapes of the grains forming the macroscopic structures of chalcopyrite compounds clearly speak for kinetic aspects controlling the growth process, at least at some of its stages. These aspects have not been considered in the discussion so far and apparently have a different impact in the final morphology of the samples as a function of the elements transported in the gas phase. In turn, there seems to be at least two distinct kinetic issues to be taken into account in order to explain the observed effects. On the one hand, the annular features observed in the case of sulfide compounds could be ascribed, to a certain extent, to the formation of $Cu_{2-x}S$ phases at relatively early stages of the growth process, where there is still a fraction of the Cu in the precursor not fully consumed by the ternary compound. The role of binary Cu-chalcogenide compounds during the growth of, e.g., $CuInS_2$ thin films for photovoltaic applications is well known in the literature after the work of Klenk *et al.*[25] Binary compounds of the type $Cu_{2-x}S$ and $Cu_{2-x}Se$ drive the recrystallization occurring in multistage-growth processes and control the incorporation of gaseous species into the on-growing solid, in the form of a quasiliquid surfactant phase (at processing temperatures above 500 °C) at the edges and surfaces of the growing structures. Even when $Cu_{2-x}Se$ and $Cu_{2-x}S$ play a similar role during the process, the actual kinetics may well differ between the cases of selenides and sulfides, as becomes apparent in Fig. 6. The annular geometry observed for the case of sulfides is thus attributed to the intermediate stages of the growth controlled by the quasiliquid binaries, assisted in the present case by the fact that samples were subjected to a constant rotation (50 rrp in all cases) during the processing. A second kinetic aspect refers to the appearance of crown-shaped structures discussed above, which has been put in connection to the occurrence of twinning and

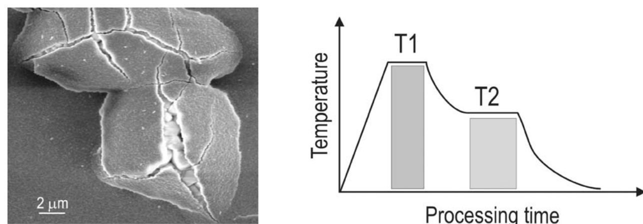

FIG. 8. (Left) $CuGaSe_2$ polycrystalline clusters, visible at the cracks, embedded in a Ga_2Se_3 matrix covering the entire substrate. Fractures of the matrix occurred presumably during cooling down as a means of release of thermal stress at those spots in contact with the ternary compound underneath. (Right) Temperature profile optimized for the sequential growth of the ternary structure (at T1) and the embedding matrix (at T2) in a single run.

stacking faults during the growth of crystallites in the characteristic tetragonal disphenoid habitus. Twinning is frequently found also in the growth of macroscopic single crystals of chalcopyrite compounds close to the nominal stoichiometry,[26,27] but seems to be ubiquitous when departing from stoichiometry toward the Ga-rich range, probably in connection to the formation of $CuGa_3Se_5$ and $CuGa_5Se_8$ phases for sufficient Ga enrichment. Interestingly, no such structures have been observed in the present work for the case of In-containing compounds, neither sulfides nor selenides (the latter not shown in Fig. 6) and might be a characteristic property of Ga-containing samples.

Figure 8 shows a SEM top view picture of the result of a growth process of type B as in Fig. 2, carried out by transporting Ga_2Se_3 on Cu at about 430 °C for about 45 min, in which chalcopyrites were grown embedded in a matrix of a binary compound. The image shows the presence of clusters of the ternary compound, whose dimensions lie in the range of some tens of micrometers, which appear coated by a thin overlayer of the binary chalcogenide. Fractures of the coating are readily visible, like the result of thermal stress while cooling the sample down after completion of the CVD process. The presence of cracks in the matrix is a fortunate occurrence for the sake of characterization, clearly revealing the presence of two distinct crystalline phases, but might, however, pose a question mark on the applicability of the approach with respect to a full embedding of the active material. Optimization of type-B process was accomplished by introducing temperature profiles during the growth process, as schematically shown in Fig. 8 (right), in such a way as to grow stepwise the ternary structure at an elevated temperature T_1 and subsequently the embedding matrix at a lower T_2. This T-optimized process resulted in closed, homogeneous embedding layers.

Not-optimized (constant temperature) type-B processes were tested also on nanometer-sized Cu precursors. By means of grazing-incidence XRD performed on such a sample [Fig. 9(A)], we could identify Ga_2Se_3 as the main crystalline phase, in addition to Mo from the substrate, thus confirming the nature of the matrix compound. Figure 9(B) shows an enlarged view around the dominant peak of Ga_2Se_3, actually composed of a doublet of peaks stemming from $\bar{1}31/200$ and $\bar{1}12/002$ reflections within a 2θ separation below 0.06°, according to the corresponding JCPD card. The feature around 28.3° has been fitted using two different Pearson VII contributions, which have been assigned to the Ga_2Se_3 reflections mentioned above and to the 112 reflection from the embedded $CuGaSe_2$ structures, showing up as a small shoulder at lower 2θ angles [shaded area in Fig. 9(B)]. Similar results were obtained from In_2S_3 transport on nanometer-sized Cu precursors. Figure 10 shows the corresponding XRD diffractogram obtained from such a sample, grown following this time a T optimized process. The upper panel shows the pattern obtained from the powder source used in the process, while the lower panel identifies In_2S_3

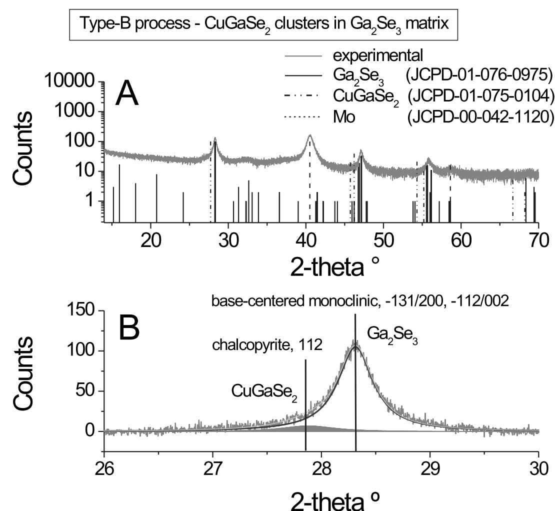

FIG. 9. (A) XRD diffractogram, realized in grazing incidence (0.7°) on a sample processed on nanoprecursors of Cu by CVD of Ga_2Se_3, to determine the nature of the matrix compound (type-B process). Peaks are attributed to Mo (substrate) and Ga_2Se_3 (matrix). (B) Enlarged range of the upper panel around the main peak of Ga_2Se_3 and corresponding fit, showing a small contribution at lower angles attributed to the presence of embedded $CuGaSe_2$ structures

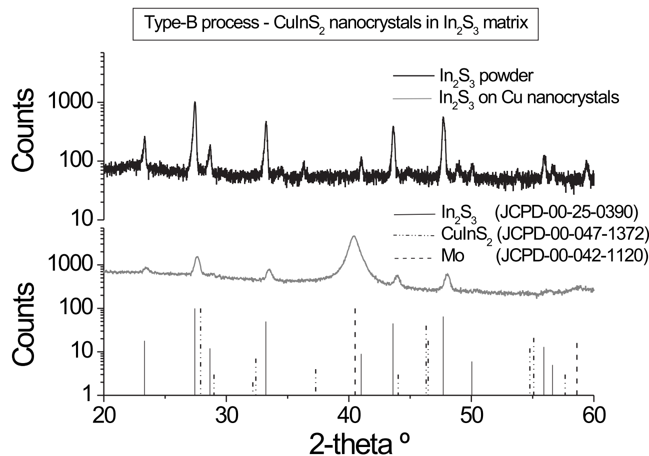

FIG. 10. (Lower panel) XRD diffractogram, realized in grazing incidence (0.7°) on a sample processed on nanoprecursors of Cu by CVD of In_2S_3 in a T optimized type-B process. The matrix compound is identified as In_2S_3, in the same crystal structure as the powder used as source material (upper panel).

FIG. 11. (Color online) (Left) STM topography (fake color, dimensions as on the right picture) image and the corresponding 3D representation (right) of a sample processed on nanoprecursors of Cu by CVD of Ga_2Se_3. Triangular crystallites correspond to the tetragonal disphenoid habitus of $CuGaSe_2$, identical to the case of isolated structures in Fig. 4.

grown on the sample as the embedding matrix, in the same crystalline phase as the powder source. These results from x-ray diffraction do thus confirm the predicted deposition of the embedding matrix of binary compounds for processes carried out at reduced temperatures, as discussed in the previous section. It was not possible, however, to identify in Fig. 10 the presence of the nanoscopic ternary compound from the XRD diffractogram, which was assumed to be fully embedded in the In_2S_3 matrix. The actual total amount of chalcopyrite material lied presumably below the limit of detection of the technique, in contrast to the case shown in Fig. 9, due to a lower density of Cu nanoparticles in the precursor.

XRD was certainly not the optimal tool for characterizing the submicroscopic structures embedded in matrix compounds, though it provided valuable information for determining the nature of the embedding layers. The reduced dimensions of the ternary nanostructures, resulting from the use of nanoprecursors, required indeed characterization tools able to resolve lateral features at nanometer scale. Figure 11 shows a scanning tunneling microscopy image taken at room temperature on a sample consisting of $CuGaSe_2$ nanocrystals in Ga_2Se_3. The sample was grown by CVD as before on Mo-coated soda-lime glass at $T_{sub}=300\ °C$, other process parameters kept the same and transferred under continuous inert gas flow to the UHV system. The typical triangular morphology of $CuGaSe_2$ tetragonal disphenoid crystallites observed in isolated structures (compare with Fig. 4) was again found in this case. Complementary information from tunneling spectroscopy was achieved simultaneously during the imaging scans by measuring $I(V)$ curves at selected spots on the sample. Following standard analysis,[28] $(dI/dV)/|I/V|$ curves were plotted, showing semiconducting behavior of the sample over the entire scanned area, characterized by the presence of a gap around the Fermi level (no tunneling current flow), confirming in turn the complete coverage of the Mo-substrate underneath. Nonetheless, distinct solid state phases could be identified, as concluded from variations in the measured band gap at different spots, corresponding to the values reported for Ga_2Se_3 ($\approx$2.4 eV) off the triangle-shaped crystallites (not shown), but differing from the expected gap value of $\approx$1.68 eV at the triangular facets ($\approx$1.82 eV, Fig. 12).

This deviation from the expected gap value was attributed to the presence of Cu-poor compositions terminating the

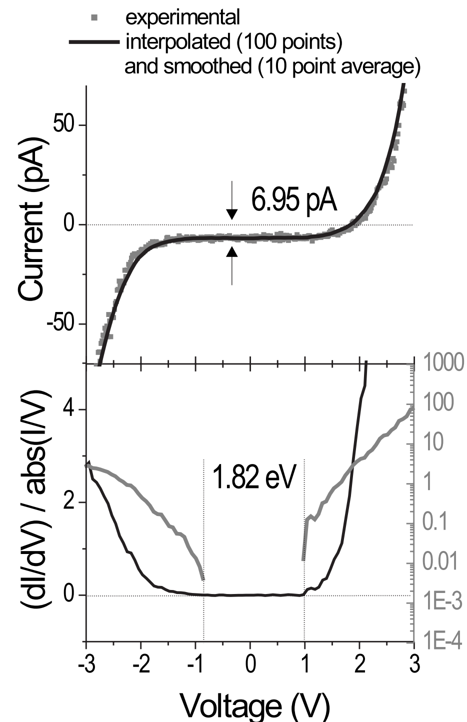

FIG. 12. (Upper panel) Scanning tunneling spectroscopic $I(V)$ curve obtained at one of the triangular features of Fig. 11. (dots: as measured and solid line: after 100-point interpolation and 10-point-average smoothing). A constant offset of 7 pA can be observed under biasing voltage probing the energy gap due to photocurrent generated from ambient light. (Lower panel) Representation of $(dI/dV)/|I/V|$ from the upper panel, both in linear (black, left axis) and logarithmic scale (gray, right axis), and corresponding energy gap.

crystallites of $CuGaSe_2$. The formation of $CuGa_3Se_5$-like phases, with a direct gap above 1.8 eV, has been reported to occur beyond the solubility range of Ga in single-phase $CuGaSe_2$ (about 20 at % off stoichiometry, see Ref. 29) and is also likely to control the surface properties of nearly stoichiometric, just slightly Cu-poor material. As commented above, these Cu-poor phases were not included in the thermochemical calculations, but their actual presence was indeed to be expected from the coexistence of $CuGaSe_2$ and Ga_2Se_3 in the embedded structures, according to the phase diagram of the quasibinary cut Cu_2Se-Ga_2Se_3.[23]

A residual amount of photocurrent, about 7 pA, constant at biasing voltages while probing the gap, was detected from the $I(V)$ curve due to ambient light present during the realization of the measurements, as can be observed in Fig. 12. The nature of this current offset at 0 V was confirmed after repeating the measurements in the dark by properly covering the windows of the analysis chamber. The extraction of measurable photocurrent (photoassisted tunneling microscopy, as termed by Grafström)[30] indicated the existence of a collecting junction. The actual location of the junction, either at the ternary/matrix interface or related to surface photovoltage developed at the scanned free surface, is considered as an issue separate from the present paper and will not be addressed here.

V. CONCLUSIONS

In summary, we have presented a simple and convenient method for the growth of highly structured materials of relevance for photovoltaic and optoelectronic applications. The method relies on the possibility of decoupling the issues of achieving a high material quality and a high degree of structuration by using precursors. Nanocrystals, polycrystalline clusters, and macroscopic dots of Cu-containing chalcopyrite material have been processed. For that purpose, Ga_2S_3, In_2S_3, Ga_2Se_3, and In_2Se_3 have been used as source materials in an open-tube CVD system, supported by halogen transport. The gaseous species were allowed to react with Cu precursors, deposited on Mo-coated glass substrates. Different distributions of the precursor have been tested, resulting in the different structures of the final product mentioned above, in what has been referred to in the text as the *structuring*. The selection of appropriate processing parameters led to the formation of highly structured ternary compounds, namely, $CuGaS_2$, $CuInS_2$, $CuGaSe_2$, and $CuInSe_2$, either as isolated structures or, alternatively, embedded in a matrix of a different semiconducting material, all in single run processes, accounting for the chemistry. Thermochemical calculations simulating the reaction processes taking place in thermodynamical equilibrium were carried out in order to predict the ranges of interest of the experimental parameters as a function of the type of process of choice. The experimental characterization of the samples grown following the proposed approach included structural and compositional analysis, in order to determine the nature of the crystalline phases present in the samples, as well as scanning probes, with lateral resolution capable of resolving nanoscopic structures. We have found differences in the fine structure of the samples that have been attributed to kinetic issues during the growth and to specific material-dependent aspects of the different compounds studied. The characterization program did support the methodology proposed. It is believed that the possibility of controlling the fabrication of highly structured materials of this type will widen their up-to-now foreseen applications.

ACKNOWLEDGMENTS

The authors gratefully acknowledge M. Kirsch and S. Wiesner for technical support, C. A. Kaufmann for operating the SEM in parts of this work, H. Mönig for support at the STM and S. Sadewasser for access to the equipment and fruitful discussions, and S. Fiechter for access to CHEMSAGE and for the fruitful related discussions. J. Kosk (University of Technology, Danzig) is also acknowledged for technical support in part of this work, in the frame of the Summer-Student Program at HMI. D.F.M. acknowledges financial support from the Helmholtz Gemeinschaft under contract "ArtSyn."

*Present address: Instituto de Energía Solar-ETSIT, Universidad Politécnica de Madrid, Avd. Complutense s.n., 28040 Madrid, Spain; dfuertes@ies-def.upm.es

[1] M. A. Green, K. Emery, D. L. King, Y. Hishikawa, and W. Warta, Prog. Photovoltaics **15**, 35 (2007).
[2] M. C. Lux-Steiner, A. Ennaoui, C.-H. Fischer, A. Jäger-Waldau, J. Klaer, R. Klenk, R. Könenkamp, T. Matthes, R. Scheer, S. Siebentritt *et al.*, Thin Solid Films **361-362**, 533 (2000).
[3] G. Itskos, R. Murray, A. Meeder, N. Papathanasiou, and M. C. Lux-Steiner, Appl. Phys. Lett. **89**, 032108 (2006).
[4] J. L. Shay, B. Tell, and H. M. Kasper, Appl. Phys. Lett. **19**, 366 (1971).
[5] S. F. Chichibu, T. Ohmori, N. Shibata, T. Koyama, and T. Onuma, Appl. Phys. Lett. **85**, 4403 (2004).
[6] Y.-J. Zhao, P. Mahadevan, and A. Zunger, Appl. Phys. Lett. **84**, 3753 (2004).
[7] *Emergence of Chalcopyrites as Nonlinear Optical Materials*, edited by R. Pandey and M. C. Ohmer, MRS Bull. 23, no. 7 (1998).
[8] D. Fuertes Marrón, A. Meeder, R. Würz, S. M. Babu, M. Rusu, T. Schedel-Niedrig, and M. C. Lux-Steiner, in Proceedings of the International Conference *"PV in Europe: From PV Technology to Energy Solution"* (WIP-Munich, Germany/ETA-Florence, Italy, 2002), p. 421.
[9] H. Peng, D. T. Schoen, S. Meister, X. F. Zhang, and Y. Cui, J. Am. Chem. Soc. **129**, 34 (2006).
[10] J. J. Nairn, P. J. Shapiro, B. Twamley, T. Pounds, R. von Wandruszka, T. R. Fletcher, M. Williams, C. Wang, and M. G. Norton, Nano Lett. **6**, 1218 (2006).
[11] M. Nanu, J. Schoonman, and A. Goossens, Nano Lett. **5**, 1716 (2005).
[12] T. Nyari, P. Barvinschi, R. Baies, P. Vazlan, F. Barvinschi, and I. Dekany, J. Cryst. Growth **275**, e2383 (2005).
[13] E. Arici, N. S. Sariciftci, and D. Meissner, Adv. Funct. Mater. **13**, 165 (2003).
[14] V. K. Kapur, A. Bansal, P. Le, and O. I. Asensio, Thin Solid Films **431-432**, 53 (2003).
[15] D. Fuertes Marrón, S. Sadewasser, S. Lehmann, and M. C. Lux-Steiner, Patent Application No. De 102006060366.4-43, Germany (pending).
[16] D. Fuertes Marrón, S. Lehmann, J. Kosk, S. Sadewasser, and M. C. Lux-Steiner, in *Thin-Film Compound Semiconductor Photovoltaics*, MRS Symposia Proceedings No. 1012, edited by T. Gessert, S. Marsillac, T. Wada, K. Durose, and C. Heske (Materials Research Society, Warrendale, PA, 2007), p. Y02-07.
[17] G. Eriksson and K. Hack, Metall. Trans. B **21**, 1013 (1990).
[18] O. Knacke, O. Kubaschewski, and K. Hesselmann, *Thermochemical Properties of Inorganic Substances* (Springer, New York, 1991).
[19] N. Meyer, Ph.D. thesis, Freie Universität Berlin, 2000.
[20] H. Watanabe, in *Halogen Transport Epitaxy*, Handbook of crystal growth Vol. 3, edited by D. T. J. Hurle (Elsevier, Amsterdam, 1994).
[21] S. Fiechter (private communication).
[22] D. Fuertes Marrón, Ph.D. thesis, Freie Universität Berlin, 2003.
[23] S. Lehmann, Ph.D. thesis, Freie Universität Berlin, 2007.
[24] H. Dittrich, Ph.D. thesis, Universität Konstanz, 1989.
[25] R. Klenk, T. Walter, H. W. Schock, and D. Cahen, Adv. Mater.

(Weinheim, Ger.) **5**, 114 (1993).
[26] Z. A. Shukri and C. H. Champness, Acta Crystallogr., Sect. B: Struct. Sci. **53**, 620 (1997).
[27] C. H. Champness, J. Mater. Sci.: Mater. Electron. **10**, 605 (1999).
[28] C. J. Chen, J. Vac. Sci. Technol. A **6**, 319 (1988).
[29] S. Fiechter, Y. Tomm, K. Diesner, and T. Weiss, Jpn. J. Appl. Phys., Suppl. **39**, 123 (2000).
[30] S. Grafström, J. Appl. Phys. **91**, 1717 (2002).